Geomorphology 395 (2021) 107971

Contents lists available at ScienceDirect

Geomorphology

journal homepage: www.elsevier.com/locate/geomorph

A mechanistic understanding of channel evolution following dam removal

Jordan Fields [a,*], Carl Renshaw [a], Francis Magilligan [a,b], Evan Dethier [a], Rebecca Rossi [a]

[a] Dartmouth College, Department of Earth Sciences, United States of America
[b] Dartmouth College, Department of Geography, United States of America

ARTICLE INFO

Article history:
Received 21 June 2021
Received in revised form 23 September 2021
Accepted 23 September 2021
Available online 29 September 2021

Keywords:
Fluvial geomorphology
Channel equilibrium
Dam removal
Sediment transport

ABSTRACT

Studies of post-disturbance recovery in alluvial channels have considered form- and/or process-based paradigms to describe pathways to dynamic equilibrium. Yet, an integrated understanding of the covariation between form and process as well as the mechanisms that drive the recovery of each remains incomplete. We used a small (4 m tall) upland dam removal in New England as a natural experiment to investigate the timing and arc of a channel's return to dynamic equilibrium conditions, using both form- and process-based perspectives. We observed rapid post-removal adjustments in the former reservoir and downstream channels, then relative stability after a 2-year flow that occurred 6 months post-removal. This pattern, previously described as the "two-phase" model of channel recovery, was the result of temporal variations in the ratio of Shields values at the 'bankfull' flow (θ_{Q2}) to critical Shields (θ_{cr}). Immediately post-dam removal, elevated sediment flux was driven by the high ratio of θ_{Q2} to θ_{cr} that resulted from decreased θ_{cr} values and elevated θ_{Q2} values. As fine-grained sediments were winnowed, θ_{cr} quickly recovered back to typical values within weeks to months. Subsequent adjustments to channel geometry by higher flows (i.e., the 2-year flow) redistributed bed shear stress and facilitated the relaxation of θ_{Q2} so that θ_{Q2}: $\theta_{cr} \approx 1$, the threshold channel criterion. Despite the rapid return to process-based equilibrium, nearly 3 years post-removal the former reservoir reach remains morphologically immature with respect to reach-scale characteristics of natural channels. Our results indicate that process-based recovery is rapid, facilitated by relatively frequent, modest flows, and dependent on the adjustment of the characteristic bed grain size (d_{50}) to reflect prevailing hydraulics. In contrast, the slower attainment of form-based equilibrium depends on the timing of less frequent flows equal to and/or larger than the bankfull discharge as well as extrinsic channel controls such as local valley topography and the availability of recruitable large wood.

1. Introduction

The morphology of alluvial river channels in humid climates disturbed by extreme discharge events is thought to adjust to a stable form over a period of years (Wolman and Gerson, 1978). However, understanding the fluvial processes that drive channel recovery and define the equilibrium form of a channel remains an ongoing challenge. Early work on the attainment of channel equilibrium postulated that stream channel shape and size depend on climatically-controlled runoff, sediment, and vegetation (Schumm and Licthy, 1963; Costa, 1974; Wolman and Gerson, 1978). In this framework, in the absence of climate change, channel recovery is evaluated as the re-attainment of a pre-disturbance channel form. Historically, researchers focused on recovery of pre-disturbance channel width to determine recovery, because of its measurement ease in the field and aerial photos (Wolman and Gerson, 1978; Simon and Hupp, 1992). Montgomery and Buffington (1997) later expanded beyond the cross-sectional perspective to use longitudinal channel reach morphology as a quantifiable metric of channel evolution and stability. Others have demonstrated that the spacing of distinctive forms, such as step-pools, pool-riffles, plane-beds, and cascade reaches, varies systematically with channel slope, width, sediment supply, and large woody debris (LWD) (Whittaker, 1987; Chin, 1989, 2002; Montgomery and Buffington, 1997; Chin and Wohl, 2005), implying that the periodicity of channel units could also be used to connote stability.

Recent work has recognized that multiple possible paths and outcomes characterize channel recovery (Phillips, 2009; Dade et al., 2011; Major et al., 2019; Renshaw et al., 2019) and thus recovery cannot always be defined with respect to a unique channel form. Further, a focus on channel form does not necessarily provide insight into the processes, and their rates, that create channel form. Moreover, the re-attainment of a stable channel morphology does not necessarily imply the re-attainment of stable channel processes such as sediment flux,

* Corresponding author.
E-mail address: fields.gr@dartmouth.edu (J. Fields).

https://doi.org/10.1016/j.geomorph.2021.107971
0169-555X/

which have been shown to vary even in the absence of changes in channel form. For example, after the catastrophic Lawn Lake Flood of 1982, Pitlick (1993) observed that after experiencing the equivalent of ~28,000 years of sediment deposition during the event, a new, stable bankfull channel was established within 2 years. Yet sediment flux remained high and variable throughout the entire five-year study period, with bedload rates at least 100 times greater than pre-flood, though few changes to the channel form resulted from higher loads (Pitlick, 1993). A similar phenomenon has been observed on the N. Fork of the Toutle River in the 40 years since the eruption of Mt. St. Helens buried that watershed (Major et al., 2019, 2020).

The apparent disconnect between the recovery of channel form and fluvial processes has redirected research focus to various process metrics, specifically the attenuation of post-disturbance sediment flux, to evaluate recovery. Recent studies using sediment evacuation following dam removals have proposed a two-phase model in which a period of high sediment flux immediately after the removal is followed by the onset of 'recovered' channel processes, during which lower average flux is punctuated by high discharge events that evacuate the remaining stored sediment (Pearson et al., 2011; Collins et al., 2017; Rathburn et al., 2018; East et al., 2018). Absent from this two-phase model, however, is an explicit explanation for how channel form evolves as process (i.e., sediment flux) varies, or vice-versa. Pfeiffer et al. (2017) suggest that channel hydraulic geometry is driven by tectonically controlled sediment flux, potentially offering a link between form and process in the two-phase model and suggesting that geometry will adjust to prevailing flux conditions. However, their idea has not yet been directly tested in the field, and it is not clear whether it accommodates rapid (<1–10 years) adjustments. East et al. (2018) adopt the framework of the two-phase model to describe channel evolution after the removal of dams on the Elwha River and show the threshold for geomorphic change is affected by sediment flux. However, their observation about variable thresholds lacks a specific hydraulic mechanism. Thus, the mechanisms responsible for the observed two-phase pattern of sediment mobility remain poorly constrained.

An implication of the two-phase model is that in some cases the time required for recovery may be set by boundary conditions extrinsic to the channel. For example, a system in which all the reservoir sediment is removed prior to dam removal should recover faster than a system where the reservoir sediment remains. Similarly, a system will recover faster from a major flood that transports most mobilized sediment during the event than from a volcanic eruption deposition without significant transport mechanisms. Schumm (1979) generalized this framework for channel response to disturbance by identifying intrinsic and extrinsic controls on channel recovery as those factors that the channel influences directly versus those that are set by extra-channel boundary conditions, respectively. The pace of recovery related to intrinsic controls is determined by channel hydraulics, including the imposed hydrology, whereas the pace of recovery related to extrinsic controls is set primarily by non-hydrologic factors.

These inter-related theories of channel recovery—the relationship between form, process, and intrinsic/extrinsic controls—can combine to provide a general theory of fluvial recovery from disturbance. With this aim, and to better describe the temporal and spatial evolution of post-disturbance channel equilibrium, here we address the following two research objectives: (1) Does the re-attainment of stable planform, and reach-scale morphologies coincide with the attenuation of elevated post-disturbance sediment mobility, and (2) what mechanisms drive the return to process- and form-based equilibrium?

To address these questions, we take advantage of the removal of a small (4 m tall) upland dam in New England as a natural experiment to evaluate what controls the trajectories of sediment transport and channel morphology as the channel re-attains a dynamic equilibrium state. We use terrestrial LiDAR and traditional survey techniques to describe the evolution of post-dam removal channel form. Process-based equilibrium is quantified using 2D hydraulic models and the deployment of novel active tracer rocks equipped with RFID (radio frequency identification) PIT (passive integrated transponders) tags and accelerometers. Together, these data allow us to investigate how the observable metrics of channel form (e.g., width, depth, cross-sectional area, channel reach types) covary with in-channel processes (e.g., shear stress, sediment mobility) and thereby delineate the processes, controls, and mechanisms that drive channels back to an equilibrium form post-disturbance. These methods integrate and augment previous work on channel recovery, linking existing, but disparate, observations of channel dimensions and sediment flux in post-disturbance alluvial channels.

2. Background

2.1. Process-based metric of equilibrium

Historically, the concept of the "bankfull" channel form has been foundational to how we understand local-, reach-, and watershed-scale stream channel adjustments. Leopold and Maddock's (1953) seminal work on hydraulic geometry power-function relationships, for example, requires a downstream comparison of flows that fill the channel to its bank tops. Similarly, in their classic papers, Leopold and Wolman (1957) and; Wolman and Leopold (1957) associate bankfull channel morphology with the processes necessary for creating and maintaining a distinct, dynamic equilibrium form. The hydrologic extension of these ideas came with Wolman and Miller's (1960) work relating the magnitude and frequency of flows that maintained the channel bankfull form to the magnitude of the flow that, over time, does the most geomorphic work (termed the effective discharge). They further found that the bankfull and effective discharges occur with a frequency commonly associated with the 1.5 to 2-year recurrence interval (RI) flood. Although this RI varies regionally and with scale (Williams, 1978), in many cases the bankfull discharge (Q_{bf}), effective discharge, and 2-year flood (Q_2) all correspond and, for a channel at equilibrium, Q_2 is just contained within the bankfull channel. Because of these inter-relationships there has always been a convenient connection in fluvial geomorphology between the effective discharge, Q_{bf}, Q_2, and an identifiable bankfull channel morphology; a connection that provides a template for characterizing the pathways and mechanisms for channel recovery to a disturbance. While agreement of Q_{eff}, Q_2, and Q_{bf} at equilibrium is not true for all hydroclimatic settings, snowmelt-dominated, gravel-bedded systems, like that studied here, generally demonstrate the best agreement between the three metrics (Doyle et al., 2007).

Mackin (1948) linked effective discharge, Q_{bf}, Q_2, and an identifiable bankfull channel morphology by theorizing that an equilibrium channel is adjusted to transport the prevailing sediment supply such that there is no net aggradation or erosion in the reach. That is, sediment flux (q_s) is longitudinally (x-direction) invariant, or at equilibrium $\frac{\partial q_s}{\partial x} = 0$. The physics necessary for this sediment balance is often assumed to depend on the Shields parameter (θ), a dimensionless ratio of bed shear stress to submerged particle weight:

$$\theta = \frac{\tau}{\left(\rho_s - \rho_f\right) g d} = \frac{hS}{Rd} \tag{1}$$

where ρ_s and ρ_f are the solid and fluid densities, g is the gravitational acceleration, d is the characteristic grain size typically taken as the median bed grain size d_{50}, h is the flow depth, S is the slope of the bed, and the relative buoyant density $R = (\rho_s - \rho_f)/\rho_f$. On the right-hand side of this equation the depth-slope product is used to approximate the bed shear stress (Leopold et al., 2020).

Using a generalized sediment transport model Dade and Friend (1998) argued that Mackin's equilibrium channel requirement that $\frac{\partial q_s}{\partial x} = 0$ implies that the Shields parameter (θ) also takes on a constant value

under the effective discharge and can therefore be used as a metric of channel equilibrium in place of sediment flux. In channels in morphometric disequilibrium, however, the assumption that the effective discharge is similar to the bankfull discharge may be problematic. Hence, we assume that the effective discharge is similar to Q_2, and assign θ_{Q2} as the value of the Shields parameter at the 2-year discharge. Dade and Friend (1998) and Renshaw et al. (2019) showed that for equilibrium channels dominated by bedload transport, $\theta_{Q2} \cong$ critical Shields (θ_{cr}), the value of the Shields parameter corresponding to the onset of significant sediment transport. Roberts et al. (2020) showed that although the onset of sediment motion does not occur at a singular Shields value, θ_{cr} can be defined as that corresponding to a 50% chance of movement of the median grain size on the channel bed.

Critical Shields values typically range between ~0.03 and ~0.09 (Buffington and Montgomery, 1997; Lamb et al., 2008; Palucis et al., 2018; Roberts et al., 2020). This range is similar to the range of θ_{Q2} in bedload-dominated channels at equilibrium (Kellerhals, 1967; Dade and Friend, 1998; Parker et al., 2007; Dade et al., 2011; Pitlick et al., 2013; Trampush et al., 2014; Li et al., 2015), supporting the empirical threshold channel assumption that in a channel at equilibrium bedload transport is just initiated at the bankfull discharge or the ~1-in-2-year flow (Wolman and Miller, 1960; Wolman and Gerson, 1978; Trampush et al., 2014).

The utility of the Shields parameter lies in its covariate nature: for a given reach, it contains information about both channel bed conditions and hydraulics. In this study we assume that in bedload-dominated systems, the departure of θ_{Q2} values from θ_{cr} provides a quantitative metric of channel process disequilibrium (Renshaw et al., 2019). We therefore track the covariation in θ_{cr} and θ_{Q2} to measure changes to sediment transport dynamics on the bed and compare these adjustments to corresponding morphologic evolution.

3. Site description

Located in central Vermont in the Upper Valley of the Connecticut River, Charles Brown Brook has a humid continental climate with cold, snowy winters and warm, humid summers. Precipitation is distributed evenly throughout the year with an annual average of 937 mm (NOAA Station GHCND:USC00273850). Charles Brown Brook drains an area of ~14.8 km^2, flowing 5.5 km at an approximate average slope of 5% from ~450 m elevation in the headwaters to join Bloody Brook at an elevation of 180 m. The slope of the stream is steeper in reaches higher in the catchment; the slope of the study reach is 2.5%. The basin is typical of watersheds in the upper Connecticut River valley; the brook's headwaters are underlain by phyllite and schistose rocks mantled by zero to several meters of glacial till and by glacio-lacustrine sediments at lower elevations (Stewart and MacClintock, 1970; Ratcliffe et al., 2011). The thin alluvial cover results in a partly confined, mixed bedrock-alluvial channel (sensu Pizzuto et al., 2018).

The locus of this study (Fig. 1) is the former Norwich Reservoir Dam, built in 1928 as a water storage pond for the Norwich Fire Department. It was originally one of two dams on the stream, however, a small downstream dam was blown out in August 2011 by Tropical Storm Irene and did not exist at the time of the removal of the Norwich Reservoir Dam. The lower dam was too small (>2 m tall) and distal to have affected any of the reaches discussed in our study, even when it existed.

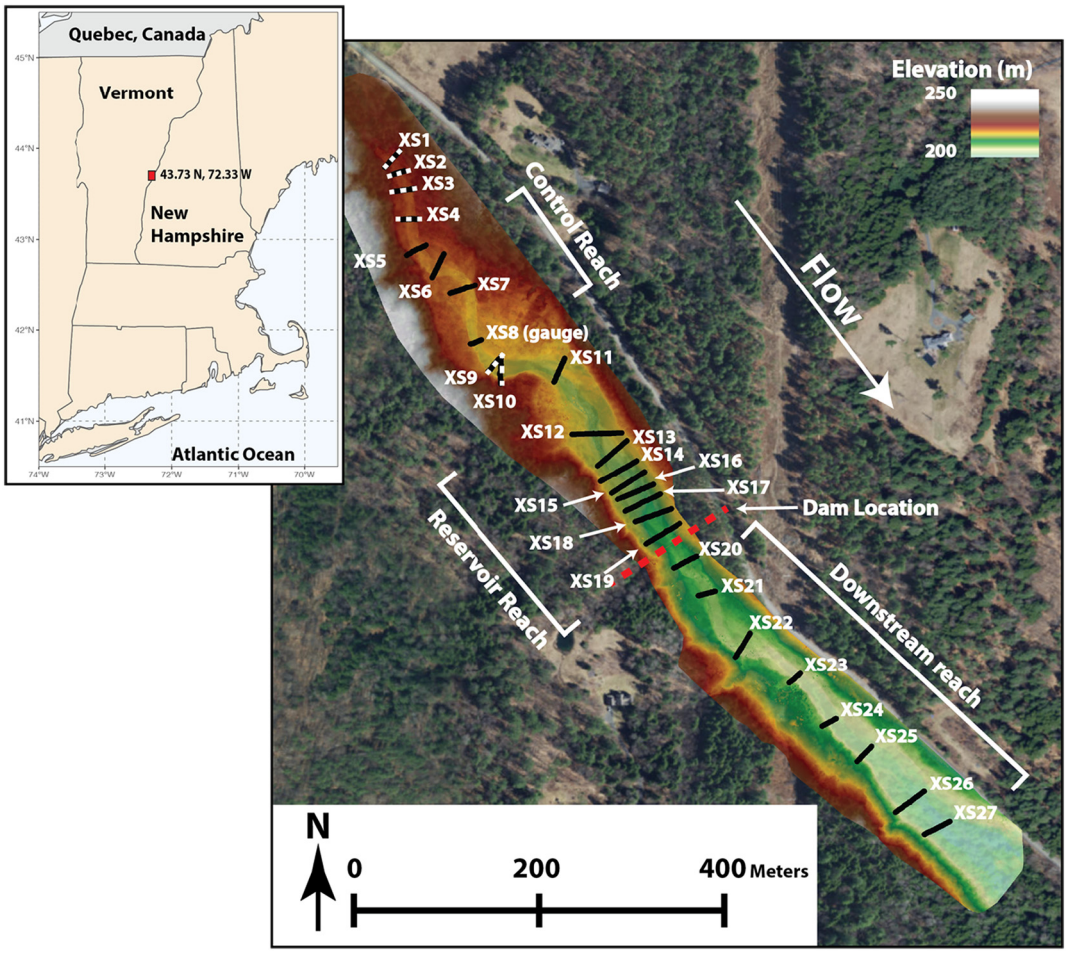

Fig. 1. Site map of the Norwich Reservoir Dam site. DEM shows TLS coverage and model extent. Total station and pebble count cross sections shown in black. Dashed cross sections are those upstream of the study reach but not used as control because of thin cover over bedrock (XS1–XS4) and the presence of a landslide (XS9 & XS10).

Prior to the removal of the Norwich Reservoir Dam, it had not been used for water supply since 1981 because of excessive sedimentation behind the dam. Previous work by Roberts et al. (2020) showed that prior to removal, dam-proximal reaches had equilibrated to the dam's presence. Critical Shields values in upstream and downstream reaches fell in the expected range (0.055 ± 0.003) even before the dam's removal and the stream regularly passed bedload over the dam (Fig. 4). The dam (4 m tall, 40 m wide, 600 m^3 concrete) and much of the impounded reservoir sediment (~8600 m^3 mechanically removed) were removed in the fall of 2018. The channel constructed post-removal (Fig. 2) was a plane-bed reach of ~3% gradient from the head of the former reservoir to the base elevation of the dam (a reach length of 120 m). Relatively few geomorphic considerations were implemented in the design of the new channel upstream of the dam and, because bank-stabilizing riparian vegetation was not planted until the spring 2019, little vegetation was present along the banks of the reach during the first year after dam removal, creating an ideal site to observe the evolution of the minimally constrained channel from a simplified state.

4. Methods

The experimental design compared the reaches most affected by the dam, particularly the former reservoir and downstream reaches, to undisturbed upstream and downstream control reaches over time. We employed a suite of geomorphic techniques to describe the morphology in each reach, including cross sections collected with a robotic total station, terrestrial LiDAR scans, pebble counts, and reach-type classifications. Together, these measurements provided a spatially extensive, high-resolution assessment of post-removal channel form over time. To evaluate sedimentologic equilibrium, we mapped the temporal evolution of Shields values at the 2-year flow (θ_{Q2}) estimated using shear stresses determined with a 2D hydraulic model. Further information about bed stability and sediment mobility was provided by tracer rocks equipped with Radio Frequency Identification (RFID) Passive Integrated Tracers (PIT) tags and data-logging accelerometers, which paired with modeled bed shear stresses, provide estimates of critical Shields (θ_{cr}) values over time. We then compared the recovery timelines of θ_{Q2} and θ_{cr} values, sediment mobility, and channel form to identify the factors that drive the evolution of each.

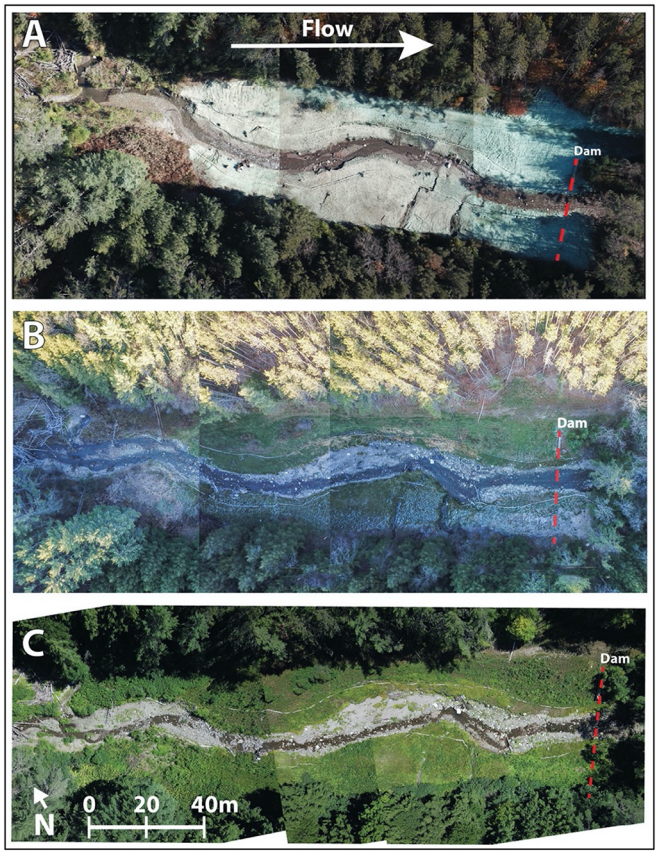

Fig. 2. Aerial images of the former reservoir area, taken with a drone, from three time periods: (A) November 2018, (B) November 2019, (C) July 2020.

4.1. Tracer rocks

We recorded bedload sediment mobility and determined θ_{cr} over the course of the channel's recovery by deploying active tracer rocks with RFID PIT tags and data-logging accelerometers ($n = 57$, 74, and 45 in 2018, 2019, and 2020, respectively). RFID chips facilitated recovery by allowing individual tracers to be located even after burial up to 1.5 m deep (Olinde and Johnson, 2015) while data logging accelerometers recorded the time of movement. An Onset HOBO U20L water level logger was installed in September 2018 to provide measurements of water stage every 5 min. These stages were subsequently converted to discharge values using a rating curve relating stage to corresponding discharge measurements made using a flow meter. Tracer movement times were matched to the hydrograph time series. We fabricated active tracers by cutting incisions into natural particles taken from the bed and gluing RFID tags into each after measuring and recording tracer dimensions along each axis. Thirty-two millimeter half-duplex (HDX) RFID tag sizes supplied by Oregon RFID were used (model HDX+ tag with 64-bit unique ID). Accelerometers were emplaced by drilling a 35 mm diameter circular hole in particles collected from the channel bed and gluing an Onset HOBO Pendant G Logger in place. The size of the accelerometer limited the minimum size of active tracers, which ranged from 60 to 112 mm (b-axis) with a median and standard deviation of 71.5 and 10 mm, respectively. Tracers were slightly larger than the median bed grain size, which varied in space and time, increasing from a median of 30 to 60 mm in the reservoir and from 15 mm to 60 mm in the downstream reach between the first tracer rock deployment in fall 2018 and summer 2020. Accelerometer fabrication decreased the density of each clast. Tracer rocks with accelerometers had an average post-fabrication density of 2180 ± 204 kg m^{-3} compared to an initial density of ~2600 kg m^{-3}. The post-fabrication density was used in the calculation of critical Shields values (Eq. 1).

Tracers were deployed in October 2018, immediately after removal. Deployment and subsequent locations of tracers were recorded using a close-range RFID antenna paired with a Trimble Geo 7× handheld GPS unit with a precision of ~1–2 m in the forested, confined valley of Charles Brown Brook. Tracers were considered to have moved if their transport distance exceeded the summed positional uncertainty of the two tracer surveys that recorded their location (generally ~1–4 m). These measurements therefore provided a conservative, lower bound for tracer mobility. Every 5 min the accelerometers recorded the direction of the gravitational vector expressed as the magnitude of each component on three orthogonal axes. The angle of rotation of the particle (ϕ) between two successive readings was determined as the dot product of the successive gravitational vectors, $\boldsymbol{a}$ and $\boldsymbol{b}$:

$$\phi = \cos^{-1} \frac{a \cdot b}{|a| \, | \, b \, |} \tag{2}$$

Angular changes <12° were considered noise as "moves" corresponding to such small changes usually did not actually correspond to real movements recorded with GPS. While the angle threshold eliminated background noise inherent in the accelerometer sensor, it also precluded the detection of "settling" movements at subcritical flows (Masteller et al., 2019). Because the tracers were painted a bright color to facilitate their recovery, they were occasionally disturbed by

passing hikers. These movements were easily detected and eliminated as those not associated with a hydrograph peak.

Tracer rocks were first deployed in the fall of the 2018 immediately after the dam was removed, resurveyed after every potentially mobilizing flow, and fully recovered and re-deployed as available memory required (~75 days). Tracers were placed carefully but not intentionally incorporated into the bed upon deployment. The tracers were removed from the channel during the winter months because of persistent ice cover at the study site.

4.2. Channel surveys

To quantify changes in channel geometry over time, we surveyed 27 cross sections using a Topcon GTS-905A total station (TS). The cross sections extended over a 1 km study section comprised of three distinct reaches: an upstream control reach unaffected by dam removal (four cross sections spaced ~40 m apart), the former reservoir (nine cross sections spaced ~20 m apart), and a reach downstream of the dam (eight cross sections spaced ~40 m apart). To extend the model boundary beyond the study reaches, four additional cross sections were established above the upstream control reach but not included in analyses. Two remaining cross sections were established in the transitional zone between the control reach and the former reservoir in a reach with a significant large woody debris jam and an active landslide scarp. Given their location in the transition zone at the head of the reservoir and these channel instabilities, these cross sections were excluded from the control reach. The final cross section (XS27) of the downstream reach was not affected by the dam removal and therefore it was used as a second control reach.

In addition to cross sections, we collected a longitudinal profile of the reach in November 2018, summer of 2019, and spring 2020. Data collected with the total station provided information about the channel bed at individual points, while spatially continuous mapping of bars, the floodplain, channel banks, and proximate hillslopes was accomplished using a Riegl VZ-400 terrestrial LiDAR scanner (TLS). The TLS creates maps of subaerial terrain with 2 cm resolution. Scans were taken at low flow to maximize the exposed area of the channel. We used these data to produce a digital elevation model (DEM) of the entire study area with a horizontal resolution of 25 cm (Fig. 1) that allowed comparison of elevation change over time by differencing DEMs in each period (Wheaton et al., 2010). For the difference of DEMs (DoD), we used a threshold filter of 10 cm, the same resolution as the DEMs. DEMs used in the DoD (10 cm) were higher resolution than DEMs used in the flow model (25 cm).

After their initial survey prior to dam removal in early fall of 2018, all cross sections were resurveyed five times post-dam removal; October 2018 immediately post-removal, November 2018 after the first significant flow post-removal, spring/summer 2019 after a 2-year flood in April 2019, spring 2020, and January 2021 after a sizable rain-on-snow event in December 2020. During each period, visual changes in the reservoir reach were recorded with drone photography (Fig. 2).

4.3. Hydraulic modeling and shields parameter calculations

To understand conditions that initiate particle motion on the bed, we developed fully 2D hydraulic models of the entire study area using version 5.0.7 of the Hydrologic Engineering Center's River Analysis System (HEC-RAS) (Brunner, 2016). We used a 25 cm horizontal resolution DEM created from a mosaic of TLS scans covering the entire study reach to define the model topography. Terrestrial LiDAR scans were taken at low flow and thus capture nearly all of the bed variability as deep pools are uncommon in the study area.

We constructed models for three periods: October 2018, November 2019, and April 2019. A model was not created for spring 2020 or 2021 because topographic differences from the previous surveys were minimal. The October 2018 model represents conditions immediately post-removal. The November 2018 model represents the channel after the first moderate flow post-removal. The April 2019 model represents the channel after the 1-in-2-year flood in the same month. For each period, model upstream boundary conditions were set with non-steady flow hydrographs that simulated a range of flows from the lowest that mobilized tracer rocks, ~ 0.2 m^3/s, to the 2-year discharge (Q_2), ~6.5 m^3/s. Q_2 was determined using the US Geological Survey's Stream Stats tool (Ries III et al., 2017) and corroborated by the geomorphic assessments of the active channel cross-sectional area in the control reach. Downstream boundary conditions were set using the normal depth condition with a friction slope of 0.01, corresponding to the channel slope at that location. Manning's roughness for each model was calibrated by matching modeled velocities and average depths to those measured at eighteen cross sections during a moderate (1.23 m^3/s) flow event in April 2020. We ran the model at a range of Manning's n values from 0.03 to 0.1 and calculated the fractional error in average depth (h) and velocity (v). Velocity and depth fractional errors were then summed to determine the value of Manning's n that minimized total error. This value, 0.045 s $m^{-2/3}$, was used in all subsequent model simulations, following the analyses of Roberts et al. (2020) of a model for the same stream reach, which showed that optimal modeled roughness remained approximately constant at flows >10% of bankfull. The majority of mobilizing flows we observed were greater than this criterion. Our sensitivity analysis showed near minimum summed error values for $n = 0.040–0.050$, therefore, we used an uncertainty in Manning's n of $\pm$0.005 s $m^{-2/3}$ and ran models with roughness coefficients of 0.040, 0.045, and 0.050 s $m^{-2/3}$ for each model period to determine a range of possible shear stresses.

We used modeled values of bed shear stress (τ) throughout the reach to calculate channel Q_2 Shields (θ_{Q2}) and critical Shields values (θ_{cr}) using Eq. (1). For θ_{Q2} calculations, we used the average shear stress at each cross section (Fig. 3), assumed a constant particle density of 2650 kg/m^3 and used the median particle size (d_{50}) at each cross section. Total uncertainty in these values reflects the range in possible shear stress values and grain size uncertainty ($\pm$12%) propagated through Eq. (1) following standard error propagation methods.

To avoid using tracer settling movements at sub-threshold flows to calculate θ_{cr}, shear stresses used in θ_{cr} calculations were determined by identifying the first storm that mobilized a majority of accelerometer-equipped tracers. The time of the first move of each tracer in that storm, as indicated by the accelerometers, was then matched with the hydrograph to determine the corresponding discharge that moved the rock. The model was run at each identified mobilizing discharge and shear stress values were extracted and averaged over a circle of 1 m radius surrounding the location of that tracer.

This method may not truly reflect a natural cobble's first movement at a threshold flow, as the tracer had not been incorporated into the bed matrix. However, using the first detectable, storm-associated tracer movement minimizes error with respect to the tracer's exact location (which is unknowable after the first move until its location is resurveyed). Therefore, we accept these critical shear stress values as lower bounds for mobility and present an average θ_{cr} value for the entire reach in each period rather than individual values determined from each tracer. All of our field data, model data, and calibration documentation is available at CUAHSI's HydroShare online database (http://www.hydroshare.org/resource/ae0589f6a2e54effb5514d126ecb6908).

4.4. Grain size and reach classification

Bed grain size was determined using Wolman pebble counts (Wolman, 1954). At least 100 clasts were measured at each cross section, in a regular pattern of twenty clasts at each of five transects located respectively at three meters upstream, one=meter upstream, at the

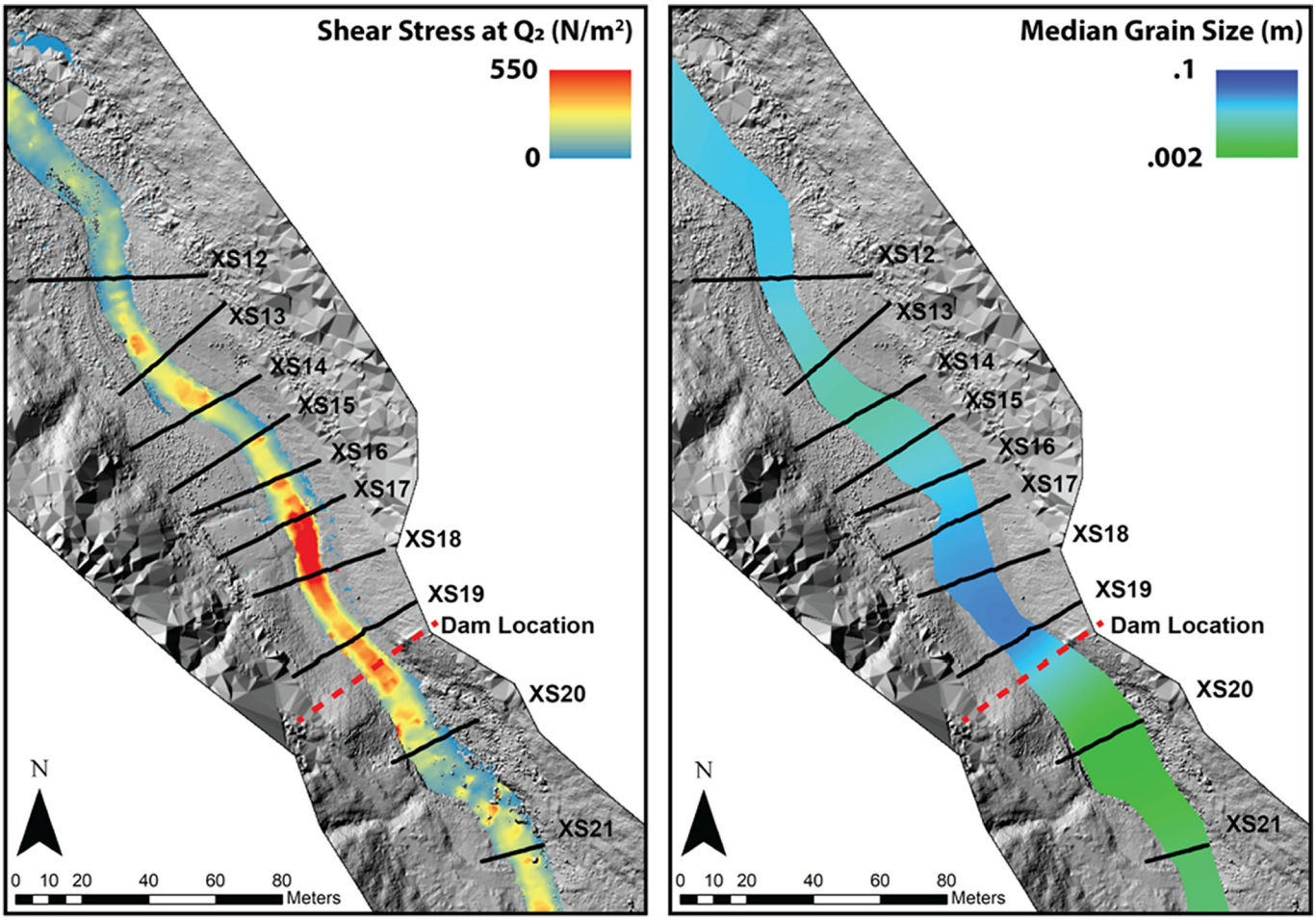

Fig. 3. Shear stress at Q2 and grain size rasters used to calculate Shields values. Reservoir reach shown. Rasters displaying values for the October 2018 (immediately post-removal) model.

cross section, 1 m downstream, and three meters downstream. All clasts with a b-axis < 2 mm were recorded as sand. An uncertainty of ±12% was applied to all grain size measurements following Wohl et al. (1996). Pebble counts were conducted at four cross sections in the reservoir reach and all eight downstream cross sections in the fall of 2018. Coverage at this limited number of cross sections was because of seasonal time constraints (i.e., ice cover). In the summer of 2019, pebble counts were completed at all cross sections and measured for the first time in the upstream reach. Summer pebble counts from the upstream, unaffected reach were also applied to the fall period because of the absence of transporting flows between survey dates. For the four additional cross sections added in the reservoir after pebble counts were completed in the fall of 2018, we used linear interpolation to estimate the median grain size for these cross sections in that period. These methods allowed us to create a complete grain size record for the calculation of Shields values throughout the reach in all time periods (see Section 4.3).

Reach classifications (Montgomery and Buffington, 1997) were completed in the reservoir and upstream reaches in the summers of 2019 and 2020. The transition between reach types was recorded with a GPS point so that step-pool spacing and the boundaries and lengths of various reach types could be compared over time.

5. Results

5.1. Tracer mobility and critical shields values

Tracer rocks tagged with accelerometers recorded sediment mobility in four periods. During 2016–2017, prior to the dam removal, Roberts et al. (2020) recorded mobility using passive tracer rocks outfitted with RFID chips but without accelerometers. Using their passive tracer data, in reaches above and below the dam they calculated an average pre-removal critical Shields value of 0.055 ± 0.003. This value is similar to those measured elsewhere in undisturbed reaches having similar slopes (Palucis et al., 2018).

In November 2018, 3 weeks after the dam removal, 91% (52 of 57) of the accelerometer-equipped tracers were mobilized by a flow significantly below Q_2 (1.42 m^3/s; $Q/Q_2 = 0.22$; Fig. 4A). All tracer rocks were recovered after this event. The average critical Shields values in all reaches during the November 2018 event (0.012 ± 0.001) was significantly lower (two tail *t*-test $p = 0.008$) than the pre-removal average (Fig. 4B). Sediment flux during this storm was markedly high relative to the modest magnitude of the discharge, eroding >500 m^3 of material even after >8000 m^3 of stored sediment was mechanically removed during dam removal.

In mid-April 2019, 6 months after the dam removal, a discharge equal to the 2-year recurrence interval discharge ($Q/Q_2 = 1.0$) caused significant mobilization. Eighty-six percent (64 of 74) of deployed accelerometer-equipped tracer rocks were recovered after this storm. Of the recovered tracers, 92% ($n = 59$) had been mobilized, with many of those downstream of the former dam buried >1 m beneath the bed surface by the >650 m^3 of sediment that eroded from the reservoir reach during this event. The average critical Shields value in the former reservoir and downstream during this event was 0.048 ± 0.003, nearly the same as its pre-removal value.

For the remainder of the study period, only limited mobility occurred. No events mobilized >25% of tracers after the April 2019 Q_2 discharge, and no events mobilized tracers beyond our positional

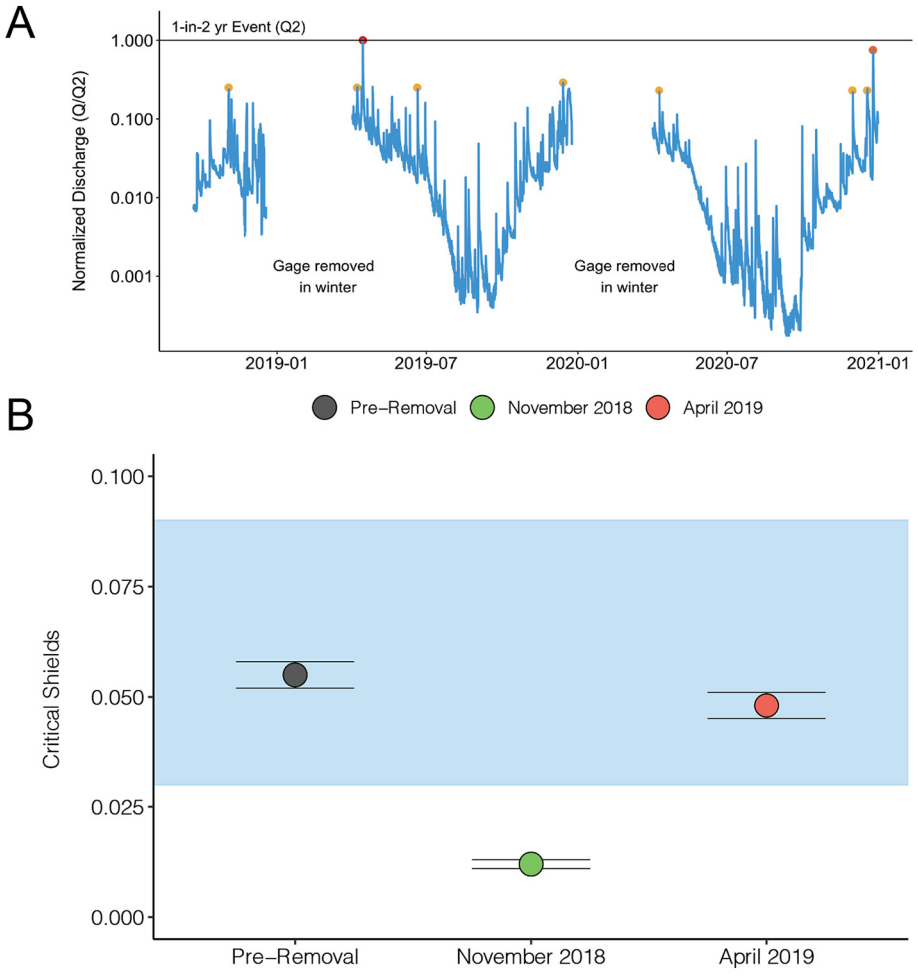

Fig. 4. (A) Normalized hydrograph from Charles Brown Brook for the entire study period. The April 2019 Q_2 event is marked in red while paired storms of 1.4 m^3/s are marked in yellow. The Christmas 2020 flood (5.2 m^3/s; 80% of Q_2) is marked in orange. (B) Critical shields values obtained from active tracer rocks plotted over time. Error bars represent standard error. The storms of equal magnitude to the November 2018 storm caused only limited mobility in 2019 and 2020, providing a lower bound for critical Shields but no further information, limiting our ability to precisely determine θ_{cr} beyond spring 2019. No tracers were deployed during the Christmas 2020 storm because of ice cover. Blue region represents expected range of θ_{cr} for gravel-bedded channels at equilibrium. (For interpretation of the references to color in this figure legend, the reader is referred to the web version of this article.)

uncertainty. The lack of mobility was in part caused by the lack of storms in that period. The largest flow between April 2019 and December 2020 was $Q/Q_2 = 0.26$, although flows of this magnitude occurred five times in that 18 month period (Fig. 4A). One larger flow of 5.2 m^3/s ($Q/Q2 = 0.8$) occurred on Christmas Day 2020, though no accelerometer-equipped tracers were deployed at this time because of thick ice cover.

While the lack of flow events after April 2019 precludes directly measuring θ_{cr}, matched flows of ~1.4 m^3/s ($Q/Q_2 = 0.22$) during which tracers were deployed in November 2018, early-April 2019 (a flow prior to the Q_2 flow in mid-April 2019), June 2019, December 2019, and April 2020, allow for a qualitative assessment of mobility and θ_{cr}. After the November 2018 storm (3 weeks post dam removal) where 91% of the tracers were mobilized by a flow of ~1.4 m^3/s, none of the subsequent flows of this magnitude (including the early-April 2019 flow just prior to the mid-April Q_2 flow) mobilized a significant (>50%) fraction of tracer rocks, despite deployment in similar locations.

5.2. Channel geometry

Major changes to channel dimensions can been divided into two periods: those changes that occurred during the modest flows immediately after the dam removal (fall-winter 2018) and those that occurred during a 2-year flood in spring 2019. Significant sediment mobility occurred during the first period, but only modest cross-sectional change. Comparing cross sections taken in October 2018 and November 2018 in the reservoir (Fig. 5), initial morphologic changes occurred primarily as minor adjustments to bed elevation and minor bank collapse and associated widening (see XS 12, 14, and 17). Sand was stored throughout the downstream reach in the fall of 2018 but was quickly exported, as recorded by coarsening d_{50} (Fig. 7C). In contrast, major adjustments to the channel's cross-sectional area occurred during the second period (Fig. 6). In particular, the upper half of the former reservoir reach (XS12–XS16) experienced significant incision (>1 m) despite substantial reservoir sediment removal during dam removal and the construction of an engineered channel. Cross sections in the lower part of the reservoir (XS17–XS19) experienced less incision (<0.25 m) on average, and the dam-proximal downstream cross sections (XS20–XS22) aggraded and widened. Downstream aggradation was persistent in these reaches proximate (<200 m) to the dam but was primarily a transient effect at XS23 through XS27, which experienced only minor changes to channel geometry over the study period (Fig. 5). Changes during the first 6 months post-removal largely set the channel's dimensions for the remainder of the study period at most cross sections, with only minor changes observed thereafter even during the December 2020 flood ($Q/Q_2 = 0.8$). We did not observe any significant changes to channel geometry in the upstream control reach over the study period or the farthest downstream cross section, XS27, which we therefore also use as an unperturbed control reach.

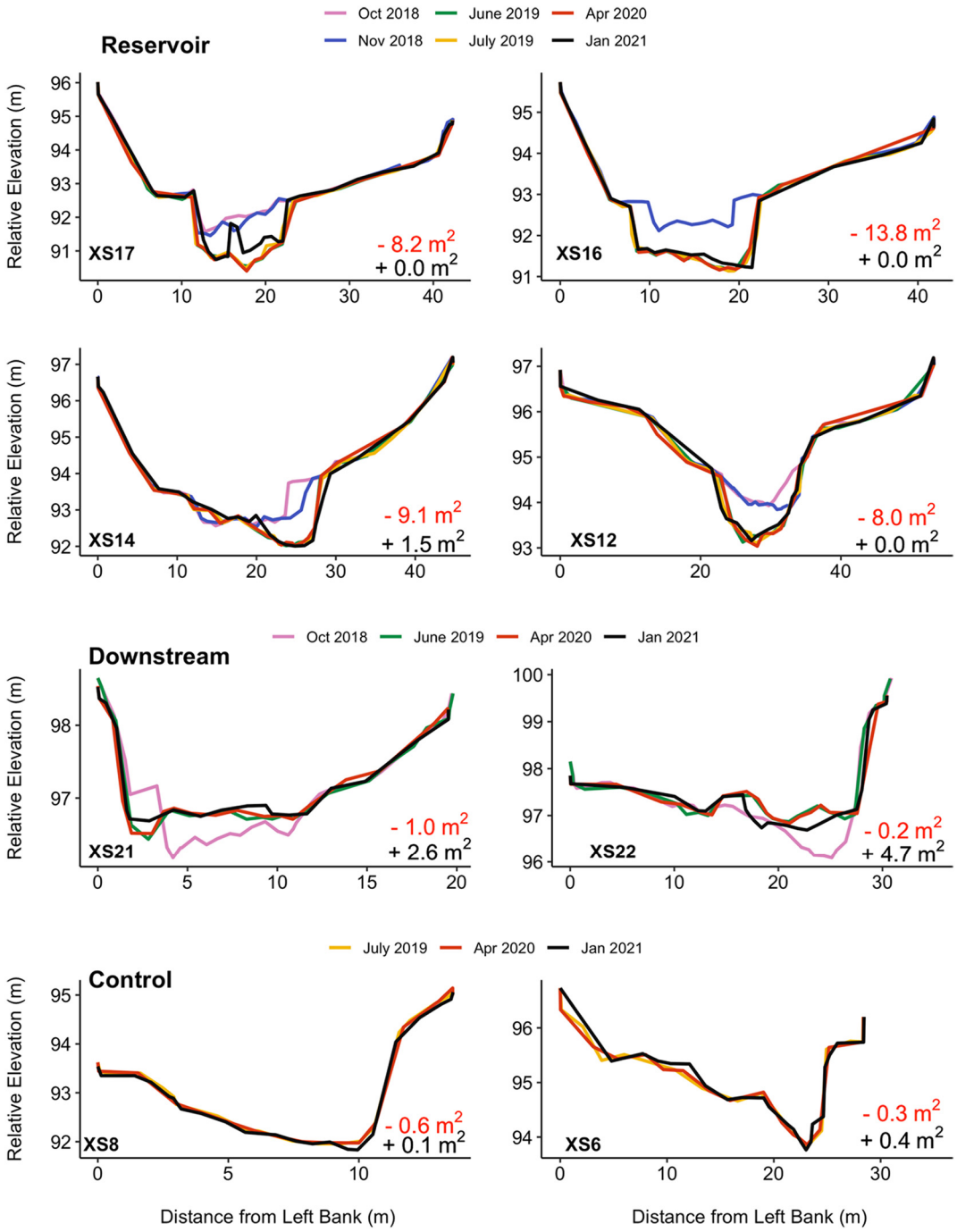

Fig. 5. Cross-sectional change between October 2018 and January 2021 in the former reservoir, downstream, and control reaches. Erosion (red) and aggradation (black) between the first and final surveys for each cross section are noted in the bottom right of each panel. Not all cross sections were surveyed in all periods because of seasonal time constraints (ice). The apparent erosion in the upstream control reaches reflects the precision of the survey method (i.e., specific survey rod placement). Qualitative observations (photos) recorded no changes in channel geometry in the control reach in any period from fall 2018 through fall 2020. (For interpretation of the references to color in this figure legend, the reader is referred to the web version of this article.)

5.3. Channel Q_2 shields

Changes in channel geometry occurred synchronously with changes in channel Q_2 Shields, θ_{Q2}, which evolved markedly between dam removal in October 2018 and the 2-year flow in April 2019, then stabilized for the remainder of the study period. Channel Q_2 Shields values were elevated immediately after the dam was removed to values much higher than the expected range for equilibrium channels (Fig. 7A). In October 2018, θ_{Q2} values averaged 0.134 ± 0.017 and 0.376 ± 0.133 (mean ± standard deviation) in the reservoir and the dam-proximal downstream reaches, respectively. In the same time period, in the control reach the θ_{Q2} average was 0.057 ± 0.012. By November 2018, one-month post-removal after the first modest matched flow event ($Q/Q_2 = 0.22$), channel Q_2 Shields values showed only minor changes in the reservoir and downstream reaches with average values of 0.143 ± 0.018 and 0.409 ± 0.159, respectively. Although unmeasured because of time and weather constraints, over the same time period the channel Q_2 Shields values in the control reach were assumed to be unchanged because repeat photography and field observations suggested that the topography and grain size

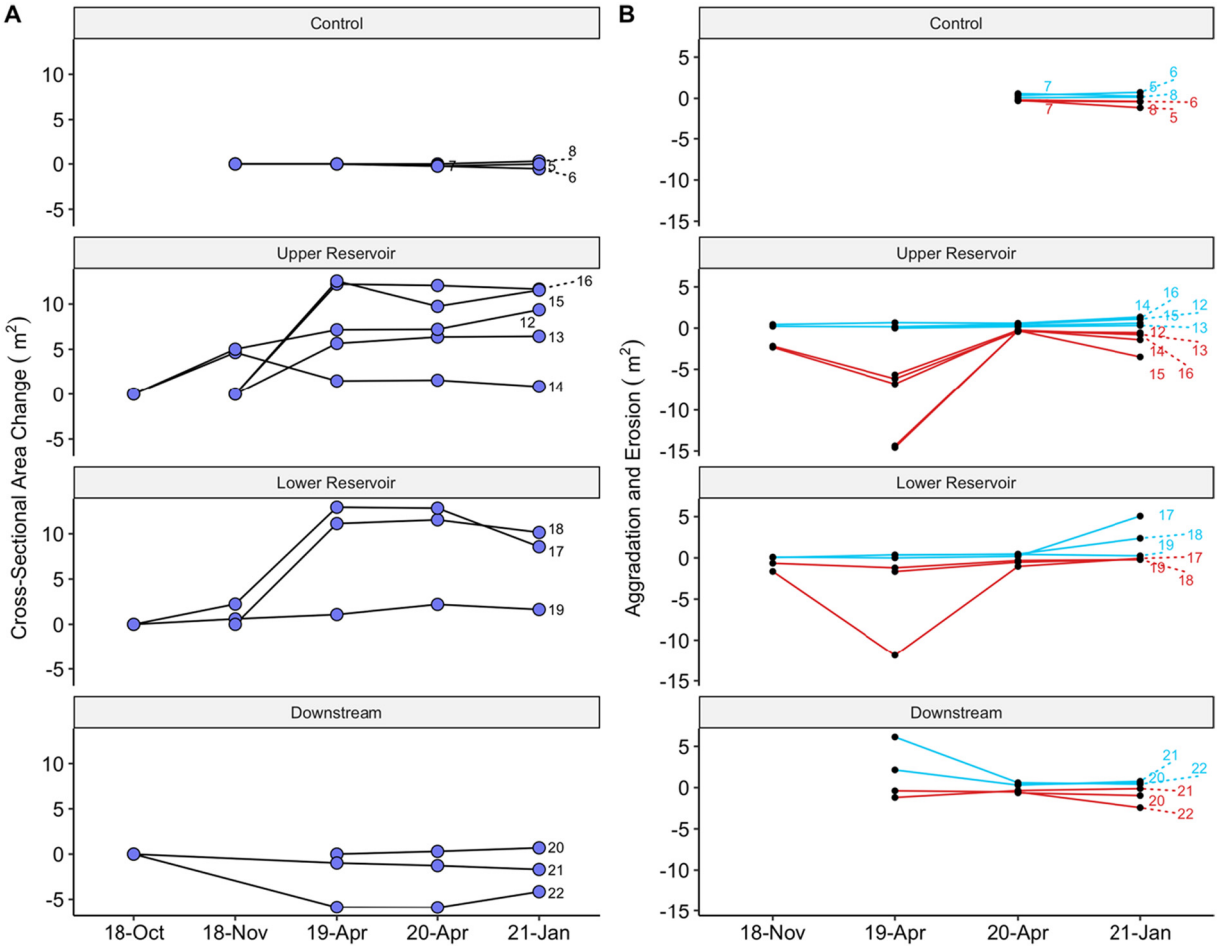

Fig. 6. (A) Change in cross-sectional area and (B) associated aggradation (blue) and erosion (red) at selected cross sections over the study period. (For interpretation of the references to color in this figure legend, the reader is referred to the web version of this article.)

data were unchanged. In the spring of 2019, after the Q_2 flow of mid-April, θ_{Q2} values dropped dramatically in the reservoir and dam-proximal downstream reaches, with averages of 0.059 ± 0.007 and 0.042 ± 0.004, respectively. Values in the control reach showed no change over the same time at 0.053 ± 0.011.

Channel Q_2 Shields values varied longitudinally throughout the reservoir and downstream reaches; within the former reservoir θ_{Q2} values were high (relative to the values in the control reach) and increased with distance downstream towards the dam, then decreased downstream of the former dam until XS27, which experienced no meaningful change in θ_{Q2} values over the entire study period (Fig. 7A). Reaches over which θ_{Q2} values were increasing in the fall 2018 period corresponded to erosional reaches while locations where θ_{Q2} values decreased over distance downstream of the former dam corresponded to aggradational reaches.

Changes in channel Q_2 Shields values resulted from covariate changes in median bed grain size and changes in shear stress driven by changes in slope, depth, and width. Relative changes in these parameters during the post-dam recovery period are shown in Fig. 7. Here the spring 2019 values of these parameters, i.e., after most of these values had stabilized, are normalized by their values immediately after dam removal in fall 2018. Overall, the greatest relative change occurred in median bed grain size, with change ratios as much as twice those of shear stress, slope, depth and width. Median grain size (d_{50}) increased universally in the former reservoir and along dam-proximal downstream reaches with change ratios of 2.05 and 10.27, respectively. In the upper reservoir, slope increased (change ratio = 1.5) while it decreased in the lower reservoir (change ratio = 0.50). Downstream of the dam, slope decreased at the cross sections most proximate to the reservoir but, overall, showed little change (change ratio = 0.97). Width and depth both decreased in the upper reservoir (change ratios of 0.92 and 0.87, respectively) and increased in the lower reservoir (change ratios of 1.35 and 1.21, respectively). We observed minor increases in width and depth in the dam-proximal downstream reaches, but otherwise little change overall with an average change ratio at all downstream cross sections of 1.01 and 1.02 for width and depth, respectively. In the reservoir, slope showed an inverse change pattern with respect to width and depth (Fig. 7D) and collectively these changes are reflected in the changes in shear stress ratios. Shear stress increased in the erosional reaches in the upper reservoir (average change ratio of 1.44) and decreased (change ratio = 0.53) in the lower reservoir (Fig. 7C). Together, these observations indicate that in the reservoir the return of Q_2 Shields values to their pre-removal values was driven by (1) bed coarsening caused by winnowing, with median bed grain size of 34 mm in Fall 2018 increasing to 65 mm after the April 2019 Q_2 discharge; and (2) the redistribution of shear stress in the reservoir reach by adjustments to channel geometry (Fig. 7C).

Downstream of the former dam, reductions in θ_{Q2} were largely driven by substantial increases in the median grain size (d_{50}) (Fig. 7C). Changes to channel geometry did contribute to local reductions in θ_{Q2}, but only in dam proximal reaches (first to third transects downstream of the dam), where aggradation lasted beyond the period of the initial sediment pulse (primarily trapped by a significant large woody debris jam 200 m downstream of the dam). At all downstream reaches – except for the farthest downstream, XS27 – grain size coarsened

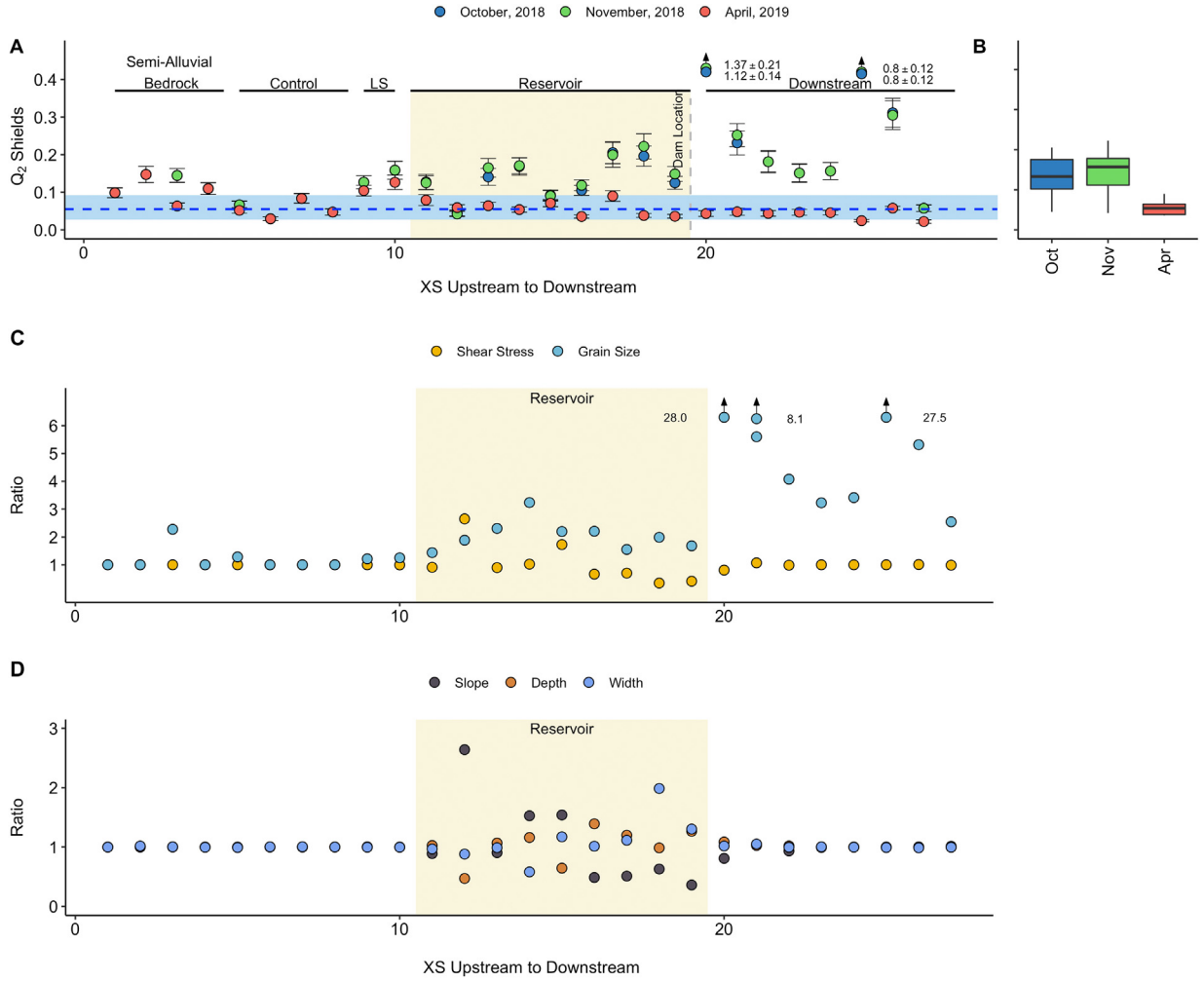

Fig. 7. (A) Channel Q_2 Shields (θ_{Q2}) values plotted at each cross section over time. Note the April 2019 values reflect topography after the 2-year flood in that month. The blue shaded region represents the "expected range" for Shields values in bedload channels. The dotted blue line represents the pre-removal critical Shields value. 'LS' denotes a reach affected by a landslide. (B) Mean θ_{Q2} values and quartiles in each period. (C) Ratios of shear stress and grain size comparing change over time by dividing values from spring 2019 by fall 2018, the period with the greatest change. (D) Ratios of width, depth, and slope over the same period. Note that the range of the ratio in (D) is half that in (C). (For interpretation of the references to color in this figure legend, the reader is referred to the web version of this article.)

significantly as fine-grained material from the initial sediment pulse was winnowed away. The median grain size (d_{50}) in downstream reaches in the fall of 2018 was 14.5 mm and 57 mm by spring 2019 (post-April storm).

5.4. Reach scale morphology

Pools in the upstream control were spaced, on average, every 2.0 and 1.9 channel widths in summers 2019 and 2020, respectively (Table 1), matching previous studies of stream morphology in forested mountain catchments, which report average pool spacing of less than one to four channel widths, with a mode between one and two (Chin and Wohl, 2005). In the reservoir, pools were spaced on average every 22.5, 3.9, and 3.5 channel widths in fall 2018, summer 2019, and summer 2020, respectively. In the reservoir reach, no reach types were formed by large woody debris (LWD) whereas over half (56%) of pools in the upstream control were LWD-forced.

Table 1
Pool-spacing data for the Norwich Reservoir Dam site on Charles Brown Brook over the two-year study period.

	Control		Reservoir		
	2019	2020	2018	2019	2020
Pool-to-pool distance (m)	21	19	207	44	39
Avg. channel width (m)	10.2	10.2	9.2	11.2	11.2
Avg. wavelength	2.04	1.86	22.52	3.94	3.45
% LWD forced	56	56	0	0	0

6. Discussion

6.1. Channel evolution governed by intrinsic controls

Schumm's (1979) description of geomorphic controls provides a useful framework for understanding the mechanisms dictating the style and tempo of post-removal channel evolution. Schumm framed channel evolution as a product of intrinsic and extrinsic controls. Following Schumm, we define intrinsic controls as those factors that can be adjusted via hydrology, such as grain size, whereas extrinsic factors are those imposed on the channel unrelated to hydrology, such as valley topography and LWD growth and recruitment. Here, we consider channel evolution through the lens of intrinsic and extrinsic controls to explain the type and timing of adjustments to channel form and processes that occurred rapidly post-removal and those that are ongoing.

Post-removal, we observed that the timing of channel adjustment and sediment mobility was influenced by the intrinsic threshold for

geomorphic change imposed by channel bed texture, which was initially low, but progressively increased following removal. At first, critical Shields was low in former reservoir reaches, because of remaining reservoir sand and silt (Wilcock et al., 2001), resulting in a highly mobile bed even at moderate flows ($Q/Q_2 < 1$). During the November 2018 flow that was only 20% of Q_2, we would have expected only limited mobility in an equilibrium channel with $\theta_{cr} \cong \theta_{Q2}$; instead, we observed almost complete mobility of deployed tracer rocks (see Section 5.1 and Fig. 4A). During this and other modest flows in Fall 2018, sand- and silt-sized reservoir sediments were winnowed from the bed and the median grain size increased, increasing the threshold for motion on the bed and therefore θ_{cr} (Wilcock et al., 2001; Masteller et al., 2019). As critical Shields increased, the near-continuous bed mobility in the weeks to month(s) post-removal ended after the fall of 2018. Contrasting with near-total mobility during the modest ($Q/Q_2 = 0.22$) November 2018 storm, no tracers moved during similar flows in early April 2019. Thus, even before the Q_2 flow of mid-April 2019, θ_{cr} values had recovered from a post-removal mean of 0.012 ± 0.001 to 0.048 ± 0.003, nearly matching pre-removal values and increasing the intrinsic threshold for adjustment beyond the capacity of modest flows. Notably, throughout this first period of the channel's evolution (dam removal to the Q_2 flow in mid-April 2019), θ_{Q2} values remained high (0.1–0.3), well above the expected range of 0.03–0.09 (Fig. 7A, B), indicating that the channel was undersized with respect to Q_2. Because of the modest channel geometry changes during this first period, the channel Q_2 Shields values were largely unaffected (Fig. 4A).

After the initial winnowing of fine sediment and consequent increase in θ_{cr}, further geomorphic adjustment of the channel required flows sufficient to mobilize bed sediment larger than sand, such as d_{50}. The timing of such adjustment is determined by the arrival of a flow capable of moving these larger grains. At our study site, a 2-year flow, sufficient to move d_{50}, occurred in mid-April 2019, 6 months after the dam was removed. During the Q_2 event, channel Q_2 Shields values were reset to the equilibrium range so that $\theta_{Q2} \cong \theta_{cr}$ (Fig. 7A,B). Our analyses show that θ_{Q2} recovery was driven primarily by coarsening grain size and shear stress redistribution caused by changes in channel geometry (Fig. 7C). This 2-year flow exceeded the required intrinsic threshold (transporting d_{50}) and rearranged the channel to accommodate similarly sized flows without further adjustment. In other words, the effective flow (Q_2), reset active channel dimensions (Fig. 7D) establishing bed shear stresses just sufficient to initiate bedload transport at Q_2, a pattern previously observed in flume settings (Pitlick et al., 2013). The stability of the channel at flows less than Q_2 after the arrival of the 2-year flow was evidenced by the only minor changes in channel cross sections during the December 2020 flood ($Q/Q_2 = 0.8$).

The 2-year flood in April 2019 imbricated framework (>250 mm) clasts, but dam-affected reaches in the former reservoir and downstream have yet—as of summer 2021—to develop well-organized, characteristic morphologic features of alluvial channels, e.g., steps, pools, riffles, and plane-bed reaches. Incipient characteristic reach types do exist in the reservoir reach (Table 1), but they are irregularly and widely spaced relative to the upstream control reach and relative to the spacing typically observed in similarly steep bedload dominated streams (Montgomery and Buffington, 1997). The relative immaturity of reservoir reaches is also marked by the disorganization of steps, which are composed of just a few framework clasts; only local imbrication of large grains; and the discontinuity of the individual steps across the stream's width.

Undeveloped reach morphologies reflect the progressive increase in the intrinsic threshold imposed by the grain size required to create these features. While the April 2019 2-year flow provided the beginning framework for development of reach-scale bedforms, larger flows are required to transport and rearrange large framework clasts (e.g., grains larger than d_{84} or even d_{95}) into organized steps. Because such flows are inherently rare, it takes longer to overcome the intrinsic threshold of transporting framework-sized grains and develop mature, 'equilibrium' reach morphologies than to stabilize the channel bed and cross section. Previous studies have reached similar conclusions, showing that one- to five-year recurrence interval flood events are capable of forming characteristic bedforms, but these bedforms may be overwritten by more rare events (30- to 50-year recurrence interval) with reach-scale channel bedforms largely reflecting the legacy of the larger floods (Hayward, 1980; Lenzi, 2001). Thus, the value of Schumm's intrinsic control framework in the context of channel evolution is that various stages of adjustment can be predicted based on the recurrence interval of flows capable of transporting progressively increasing grain sizes.

6.2. Channel evolution governed by extrinsic controls

The intrinsic control of grain size does not alone determine the timing of stable channel evolution. Our results indicate that while the timing of channel adjustment partially results from the timing of flows sufficient to overcome successively greater intrinsic controls related to the mobility of relevant grains sizes (fine-grained reservoir sediments, then bed d_{50}, and finally framework clasts), other aspects of channel adjustment are dictated by extrinsic controls. For example, the discharge required to fill the channel banks (i.e., Q_{bf}) varies widely among cross sections; because of the incision in the upper reservoir, generally $Q_{bf} \gg Q_2$ (Fig. 8). Because streams at equilibrium have banks heights that are generally reached by Q_2 (Trampush et al., 2014), full channel adjustment at the Norwich Reservoir Dam remains incomplete. Such adjustment requires continued bank undercutting, subsequent collapse, and transport of remaining legacy sediments from the reservoir until $\theta_{bf} \cong \theta_{Q2} \cong \theta_{cr}$. In contrast to adjustments to sediment flux and active channel dimensions, the continued evolution of a channel connected to the floodplain at the Q_2 flow is controlled by spatially variable extrinsic controls set by, in this case, the remnant reservoir sediment and possibly the cohesion of banks sediments (Dunne and Jerolmack, 2020).

Similarly, reach morphologic adjustment also appears to be limited by the extrinsic control of LWD recruitment. In our reach classifications, we noted that 56% of pools in the control reach were LWD forced, whereas none in the reservoir reach were (all engineered wood additions are stranded above the active channel after incision and lateral migration). Large woody debris has been shown to be a primary control on pool formation and spacing in forested mountain streams (Montgomery et al., 1995) and likely accounts for some of the disparity in pool-spacing between the reservoir and control reaches at this site.

6.3. A mechanistic understanding of existing models of channel recovery

Our data show that primary channel evolution at the Norwich Reservoir Dam site was dictated by the intrinsic control of grain size. Early changes occurred nearly continuously as a result of modest, albeit geomorphically effective, flows, but such changes were primarily limited to the channel bed. Later changes that mobilized d_{50} and significantly altered the channel's geometry to reflect prevailing hydraulics and establish a threshold channel, required larger, more infrequent flows—namely the 2-year flood, Q_2.

The same pattern of rapid, then episodic, adjustment has been observed previously and described, first in the "channel evolution model" (Simon and Hupp, 1987, 1992), and later refined by the post-dam removal "two-phase model" (Pearson et al., 2011; Collins et al., 2017; East et al., 2018). East et al. (2018) describe the two-phase phenomenon as a result of a transition from "transport-limited" to "supply-limited" conditions. Changing sediment supply in turn affects the stream power associated with substantial geomorphic change (East et al., 2018). By specifically tracking the phased adjustment of θ_{cr} and θ_{Q2}, we provide a mechanism to explain the observed two-phase

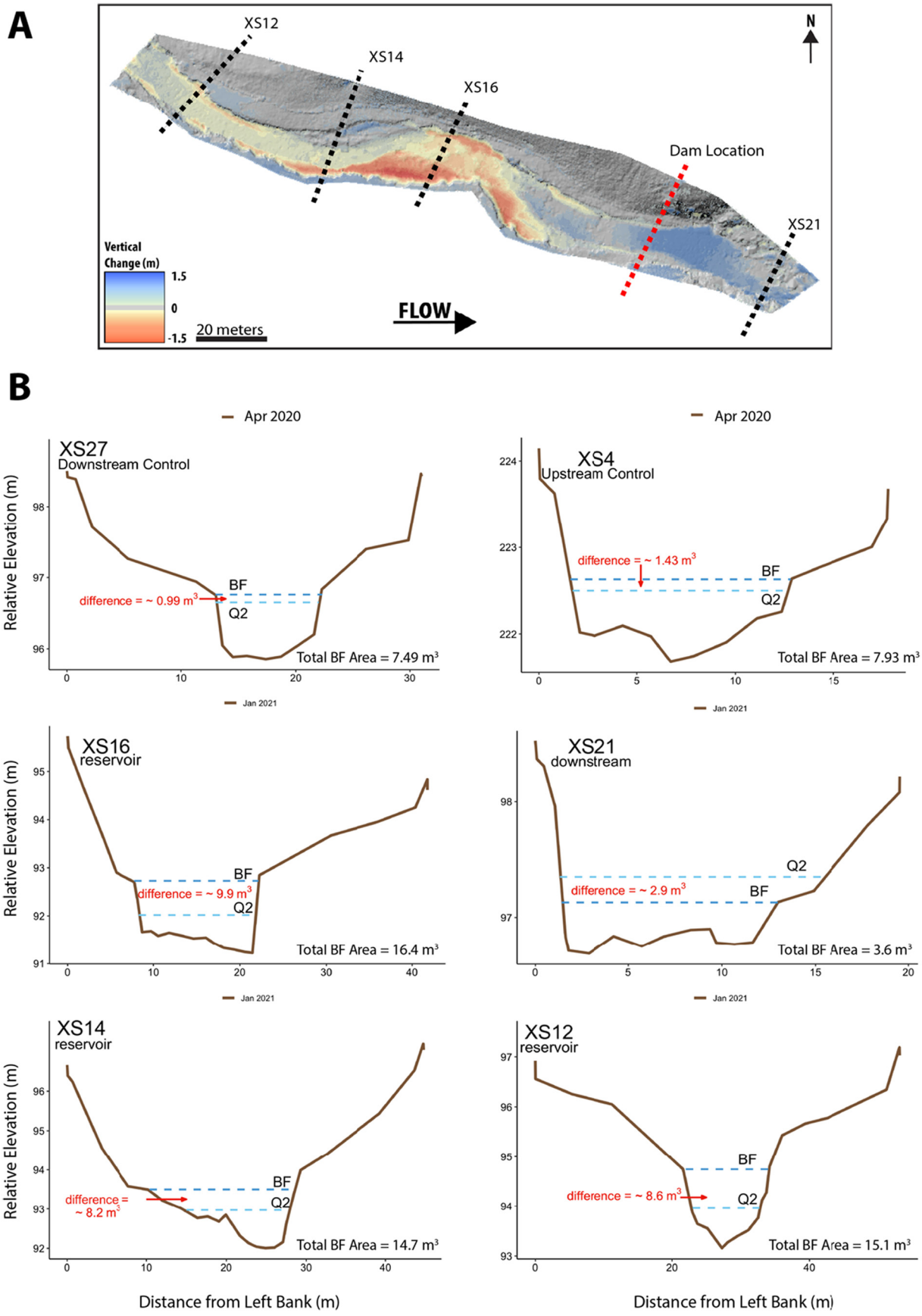

Fig. 8. A) Difference of DEMs between November 2018 and April 2019 (post-flood). B) Water surface elevations of the channel-filling flow and the 2-year flow (Q_2) at selected control (top), reservoir and downstream cross sections (lower panels). Difference in cross-sectional area between the bankfull and Q_2 flows are shown in red.

recovery behavior (Fig. 9). Post-dam removal, a period of intense sediment flux is driven by imbalanced Shields values where $\theta_{Q2} \gg \theta_{cr}$. Changes to the channel bed occur as moderate flows coarsen median bed grain size via winnowing. These bed changes rapidly (weeks to months) drive θ_{cr} to within the expected equilibrium range (a phenomenon also observed by Masteller et al., 2019). Stabilization of the bed to typical θ_{cr} values limits sediment transport by moderate flows, but θ_{Q2} values remain high; therefore, rapid, if waning sediment flux may continue. Thereafter, larger, channel-forming flows (1.5–2 year recurrence interval) are required to adjust channel geometry and d_{50} such that θ_{Q2} returns to the typical ranges, resulting in equilibrium conditions where $\theta_{Q2} \cong \theta_{cr}$. Finally, our results indicate that the evolution of energy-dissipating bedforms such as steps, pools, and riffles, occur on a much longer timescale dictated by the highest intrinsic threshold, set by d_{95+} transport thresholds, as well as extrinsic controls of LWD recruitment and full evolution of bankfull channel dimensions (Fig. 9).

Previous work has invoked sediment supply as the control on channel geometry and geomorphic evolution (Pfeiffer et al., 2017; East et al., 2018). Our findings provide a mechanism for this effect by showing that lower critical Shields values result in higher sediment flux. Like East et al. (2018), we found variable geomorphic effects of given shear stresses at unique cross sections, but we suggest that spatial variability in channel evolution results from the asynchronous recovery of critical Shields values. At first, areas where θ_{cr} remains low relative to θ_{Q2} experience high sediment mobility, even at low flows. As the disparity between θ_{cr} and θ_{Q2} declines with time, flux declines; non-uniformity in this decline can result in a seemingly heterogenous assortment of stream power thresholds.

A similar logic may also complement the pioneering work of Pfeiffer et al. (2017), who expanded beyond the cross section or reach scale to describe continental-scale trends in sediment mobility on a millennial timescale using ^{10}Be erosion rates. They invoke sediment supply as the driver of high θ_{bf}/θ_{cr} ratios in their comparison of western US rivers to rivers in eastern and intermountain regions (Pfeiffer et al., 2017). Our directly measured Shields values are a useful comparison to Pfeiffer et al.'s slope-derived θ_{cr} values (Lamb et al., 2008). At our site, the ratio of θ_{Q2}/θ_{cr} over time (Fig. 10) arcs back towards the range observed by Pfeiffer et al. (2017) at their non-West Coast sites, where $\theta_{Q2}/\theta_{cr} \approx 1$ (Pfeiffer et al., 2017, Fig. 1B). At the Norwich Reservoir Dam site, declines in θ_{Q2}/θ_{cr} over time were driven primarily by increasing θ_{cr}, as shown by the large decline in the ratio between dam removal (October 2018) and the next mobilizing event (November 2018) when θ_{Q2} did not change significantly over the same interval (Fig. 7). Thus, the pertinent effect of sediment supply on channel dynamics may be to lower (or keep low) critical Shields values via the persistent addition of sand-sized material to the channel, increasing θ_{Q2}/θ_{cr}, and thus sediment flux.

6.4. Implications for river restoration

Understanding channel evolution from the perspective of intrinsic and extrinsic controls provides insights for improving restoration in practice. The channel design implemented by engineers at Charles

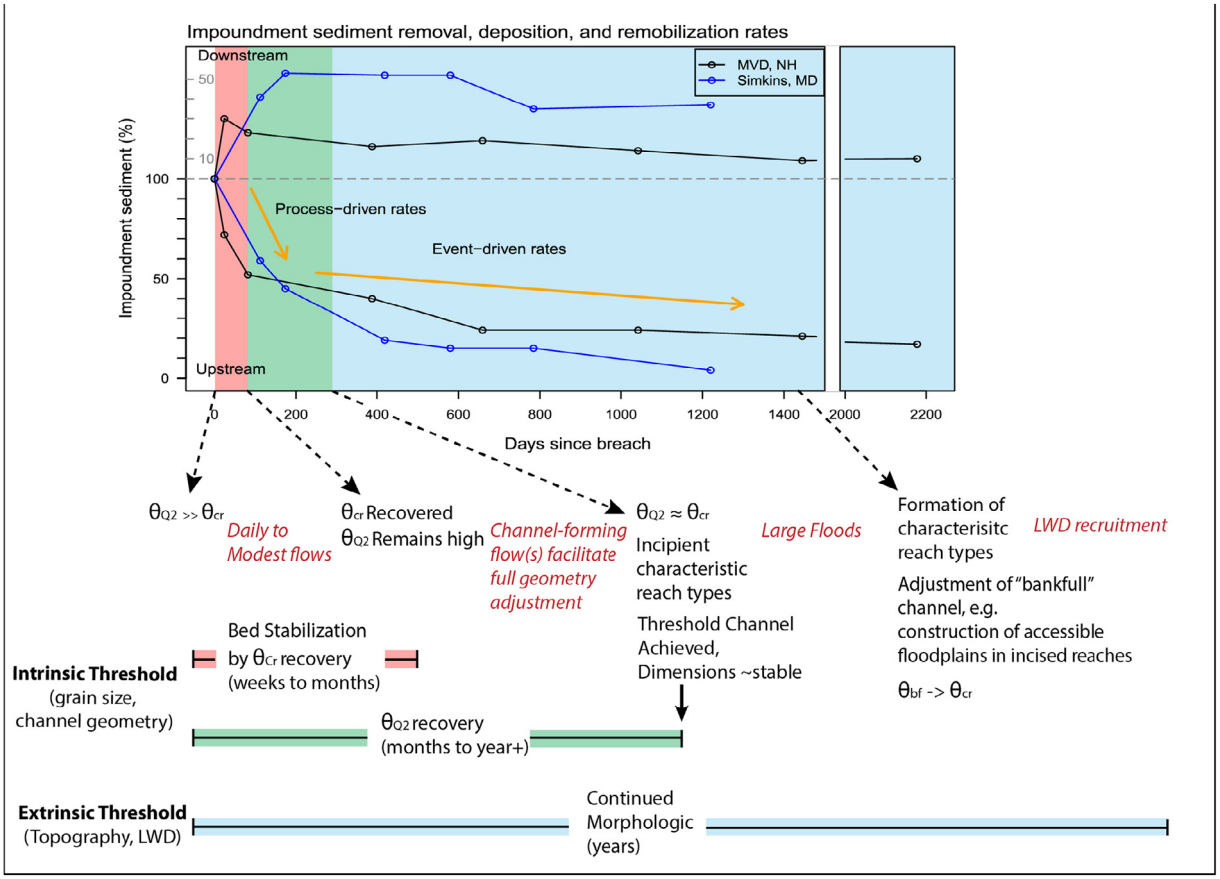

Fig. 9. Conceptual diagram of Pearson et al.'s Two-Phase model overlain by our mechanistic additions. This figure shows Collins et al.'s (2017) comparison of sediment evacuation rates at the Merrimack Valley Dam (MVD) and Simkins Dam, to which they fit a two-part exponential fit to describe the evolution of former reservoir reaches post-dam removal. Here we show that the behavior of critical and bankfull Shields values over time explain their observed two-phases and highlight the temporal disparity between form and process equilibrium. Colored regions correspond to the three phases in our model: the rapid recovery of θ_{cr} (red), followed by channel geometry adjustment facilitating θ_{bf} recovery (green), and continued morphologic adjustment to develop characteristic reach types over the following years (blue). (For interpretation of the references to color in this figure legend, the reader is referred to the web version of this article.)
Modified from Collins et al. (2017).

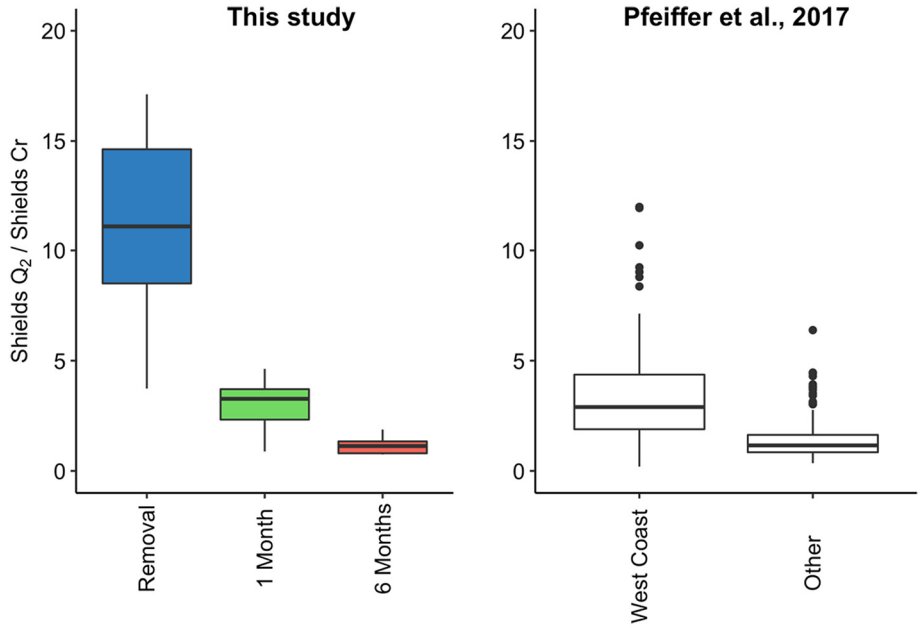

Fig. 10. (Left) The ratio of θ_{Q2}/θ_{cr} over time at cross sections in the former reservoir reach at the Norwich Reservoir dam site and, (Right) the ratio of θ_{bf}/θ_{cr} reported by Pfeiffer et al. (2017) at sites around North America.

Brown Brook was quickly overprinted, even by moderate flows, stranding LWD additions and other constructed geomorphic features. Rather than use hard engineering or channel form criteria in designing channels, our results suggest the opposite: to use process-based approaches (Beechie et al., 2010; Wohl et al., 2015; Friberg et al., 2016) in locations where appropriate, allowing for a period of natural adjustment to the prevailing hydrology (i.e., Q_2) followed later by a design that may accelerate further recovery, perhaps by the addition of wood or framework clasts as described by Wohl et al.'s (2015) "hybrid design" strategy. Our observation that recovery is contingent on the arrival of sequenced flows capable of moving requisite grain sizes suggests a novel approach in the case where a dam is being removed from a river with multiple dams. In such a case, dams might be removed systematically such that upstream dam releases are utilized to create sequenced flows that facilitate channel recovery at lower dam site(s) post-removal. Given the preponderance of dams on American rivers, channels with multiple impoundments are not uncommon. At present, proposed removals of dams on the Klamath and Lower Snake rivers in the western U.S. provide examples of sites where sequential hydrologic channel restoration might be an effective and economic strategy.

7. Conclusions

Through the novel use of modeled and observed critical and Q_2 Shields values, this study quantifies the timing and pathways of channel hydraulic and morphologic adjustments following disturbance as it strives to re-establish equilibrium. The Shields parameter offers a quantitative approach for describing the onset and maintenance of dynamic stability that does not require direct measurements of sediment flux. Instead, the departure of Q_2 Shields values from the critical Shields values during the post-removal period provides a quantitative proxy of channel disequilibrium (Pitlick et al., 2013) similar to watersheds experiencing progressive changes in sediment supply (Pfeiffer et al., 2017).

Our results show that the re-attainment of channel equilibrium post-disturbance is a spatially and temporally heterogenous process governed by the intrinsic geomorphic threshold of grain size and later by the extrinsic controls of valley topography and LWD recruitment. Framed in terms of geomorphic controls, the salient empirical observations of channel recovery described by the channel evolution model (Simon and Hupp, 1987, 1992) and the post-dam removal two-phase model (Pearson et al., 2011; Collins et al., 2017; East et al., 2018) are explained by progressive adjustments to grain size and channel geometry, reflected in critical and Q_2 Shields values. Likewise, the heterogeneous nature of channel evolution post-disturbance reflects the spatially-varied evolution of grain size with hydrology providing the necessary stream power to overcome various intrinsic controls in a given reach while also facilitating stability by raising the threshold for continued channel evolution. Final morphologic adjustment appears to be dependent on extrinsic controls outside the active channel zone and thus may take much longer than processes to fully equilibrate.

Lastly, this field and modeling based study contributes broadly to the extant literature on channel recovery and the attainment of post-disturbance equilibrium. Early work generally emphasized single-path, single-outcome trajectories as quantified using a single channel metric, most often width (Costa, 1974; Wolman and Gerson, 1978; Krapesch et al., 2011). However, width may not always be the salient geomorphic adjustment of a channel, nor should equilibrium be framed by one singular metric. Channels have multiple degrees of freedom to adjust (Hey and Thorne, 1986; Phillips, 1991) and to focus on only one of those possible modes of adjustments overlooks the range of potential adjustments occurring in other parameters. Our results emphasize the multiple degrees of freedom of channel responses whereby response and recovery are characterized by multiple possible paths and outcomes (Phillips, 2009; Dade et al., 2011).

Declaration of competing interest

The authors declare that they have no known competing financial interests or personal relationships that could have appeared to influence the work reported in this paper.

Acknowledgements

We are grateful for the help in the field from numerous undergraduates, including Isaac Freitas-Egan, Megan Clark, and Abby Wiseman. This work was partially funded by the National Science Foundation (BCS-1626414 and BCS-1951469), a Geologic Society of America

Student Grant, the Neukom Institute for Computational Science, and the Dartmouth Earth Science Department.

References

Beechie, T.J., Sear, D.A., Olden, J.D., Pess, G.R., Buffington, J.M., Moir, H., Roni, P., Pollock, M. M., 2010. Process-based principles for restoring river ecosystems. BioScience 60, 209–222. https://doi.org/10.1525/bio.2010.60.3.7.

Brunner, G., 2016. HEC-RAS 5.0 Reference Manual: US Army Corp of Engineers Computer Program Documentation. CPD-69 547 p. https://www.hec.usace.army.mil/software/hec-ras/documentation/HEC-RAS%205.0%20Reference%20Manual.pdf. (Accessed March 2020).

Buffington, J.M., Montgomery, D.R., 1997. A systematic analysis of eight decades of incipient motion studies, with special reference to gravel-bedded rivers. Water Resour. Res. 33, 1993–2029. https://doi.org/10.1029/96WR03190.

Chin, A., 1989. Step pools in stream channels. Prog. Phys. Geogr. 13, 391–407. https://doi.org/10.1177/030913338901300304.

Chin, A., 2002. The periodic nature of step-pool mountain streams. Am. J. Sci. 302, 144–167. https://doi.org/10.2475/ajs.302.2.144.

Chin, A., Wohl, E., 2005. Toward a theory for step pools in stream channels. Prog. Phys. Geogr. 29, 275–296. https://doi.org/10.1191/0309133305pp449ra.

Collins, M.J., et al., 2017. Channel response to sediment release: insights from a paired analysis of dam removal. Earth Surf. Process. Landf. 42, 1636–1651. https://doi.org/10.1002/esp.4108.

Costa, J.E., 1974. Response and recovery of a Piedmont watershed from tropical storm Agnes, June 1972. Water Resour. Res. 10, 106–112. https://doi.org/10.1029/WR010i001p00106.

Dade, W.B., Friend, P.F., 1998. Grain-size, sediment-transport regime, and channel slope in alluvial rivers. The Journal of Geology 106, 661–676. https://doi.org/10.1086/516052.

Dade, W.B., Renshaw, C.E., Magilligan, F.J., 2011. Sediment transport constraints on river response to regulation. Geomorphology 126, 245–251. https://doi.org/10.1016/j.geomorph.2010.11.007.

Doyle, M.W., Shields, D., Boyd, K.F., Skidmore, P.B., Dominick, D., 2007. Channel-forming discharge selection in river restoration design. J. Hydraul. Eng. 133, 831–837. https://doi.org/10.1061/(ASCE)0733-9429(2007)133:7(831).

Dunne, K.B.J., Jerolmack, D.J., 2020. What sets river width? Sci. Adv. 6, 1–8. https://doi.org/10.1126/sciadv.abc1505.

East, A.E., Logan, J.B., Mastin, M.C., Ritchie, A.C., Bountry, J.A., Magirl, C.S., Sankey, J.B., 2018. Geomorphic evolution of a gravel-bed river under sediment-starved vs. sediment-rich conditions: river response to the world's largest dam removal. J. Geophys. Res. Earth Surf. https://doi.org/10.1029/2018JF004703.

Friberg, N., Angelopoulos, N.V., Buijse, A.D., Cowx, I.G., Kail, J., Moe, T.F., Moir, H., O'Hare, M.T., Verdonschot, P.F.M., Wolter, C., 2016. Chapter eleven - effective river restoration in the 21st Century: from trial and error to novel evidence-based approaches. In: Dumbrell, A.J., Kordas, R.L., Woodward, G. (Eds.), Advances in Ecological Research. Large-Scale Ecology: Model Systems to Global Perspectivesv. 55. Academic Press, pp. 535–611. https://doi.org/10.1016/bs.aecr.2016.08.010.

Hayward, J.A., 1980. Hydrology and Stream Sediments in a Mountain Catchment: Lincoln College. Tussock Grasslands and Mountain Lands Institute. https://hdl.handle.net/10182/5664. (Accessed August 2020).

Hey, R.D., Thorne, C.R., 1986. Stable channels with mobile gravel beds. J. Hydraul. Eng. 112, 671–689. https://doi.org/10.1061/(ASCE)0733-9429(1986)112:8(671).

Kellerhals, R., 1967. Stable channels with gravel-paved beds. Journal of the Waterways and Harbors Division 93, 63–84.

Krapesch, G., Hauer, C., Habersack, H., 2011. Scale orientated analysis of river width changes due to extreme flood hazards. Nat. Hazards Earth Syst. Sci. 11, 2137–2147. https://doi.org/10.5194/nhess-11-2137-2011.

Lamb, M.P., Dietrich, W.E., Venditti, J.G., 2008. Is the critical Shields stress for incipient sediment motion dependent on channel-bed slope? J. Geophys. Res. Earth Surf. 113. https://doi.org/10.1029/2007JF000831.

Lenzi, M.A., 2001. Step–pool evolution in the Rio Cordon, northeastern Italy. Earth Surf. Process. Landf. 26, 991–1008. https://doi.org/10.1002/esp.239.

Leopold, L.B., Maddock, T., 1953. The hydraulic geometry of stream channels and some physiographic implications. US Government Printing Office, p. 252.

Leopold, L.B., Wolman, M.G., 1957. River channel patterns: braided, meandering, and straight. USGS Geological Survey Professional Paper. 282-B (50 p).

Leopold, Luna B., Wolman, M. Gordon, Miller, John P., Wohl, Ellen, 2020. Fluvial Processes in Geomorphology. Courier Dover Publications.

Li, C., Czapiga, M.J., Eke, E.C., Viparelli, E., Parker, G., 2015. Variable shields number model for river bankfull geometry: bankfull shear velocity is viscosity-dependent but grain size-independent. J. Hydraul. Res. 53, 36–48. https://doi.org/10.1080/00221686.2014.939113.

Major, J.J., Zheng, S., Mosbrucker, A.R., Spicer, K.R., Christianson, T., Thorne, C.R., 2019. Multidecadal geomorphic evolution of a profoundly disturbed gravel bed river system—a complex, Nonlinear Response and Its Impact on Sediment Delivery. J. Geophys. Res. Earth Surf. 124, 1281–1309. https://doi.org/10.1029/2018JF004843.

Mackin, J. Hoover, 1948. Concept of the graded river. GSA Bulletin 59, 463–512.

Major, J.J., Spicer, K.R., Mosbrucker, A.R., 2020. Effective hydrological events in an evolving mid-latitude mountain river system following cataclysmic disturbance—a saga of multiple influences. Water Resour. Res., 57 https://doi.org/10.1029/2019WR026851.

Masteller, C.C., Finnegan, N.J., Turowski, J.M., Yager, E.M., Rickenmann, D., 2019. History-dependent threshold for motion revealed by continuous bedload transport measurements in a steep mountain stream. Geophys. Res. Lett. 46, 2583–2591. https://doi.org/10.1029/2018GL081325.

Montgomery, D.R., Buffington, J.M., 1997. Channel-reach morphology in mountain drainage basins. Geol. Soc. Am. Bull. 109, 596–611. https://doi.org/10.1130/0016-7606(1997)109<0596:CRMIMD>2.3.CO;2.

Montgomery, D.R., Buffington, J.M., Smith, R.D., Schmidt, K.M., Pess, G., 1995. Pool spacing in forest channels. Water Resour. Res. 31, 1097–1105. https://doi.org/10.1029/94WR03285.

Olinde, L., Johnson, J.P.L., 2015. Using RFID and accelerometer-embedded tracers to measure probabilities of bed load transport, step lengths, and rest times in a mountain stream. Water Resour. Res. 51, 7572–7589. https://doi.org/10.1002/2014WR016120.

Palucis, M.C., Ulizio, T.P., Fuller, B., Lamb, M.P., 2018. Flow resistance, sediment transport, and bedform development in a steep gravel-bedded river flume. Geomorphology 320, 111–126. https://doi.org/10.1016/j.geomorph.2018.08.003.

Parker, G., Wilcock, P.R., Paola, C., Dietrich, W.E., Pitlick, J., 2007. Physical basis for quasi-universal relations describing bankfull hydraulic geometry of single-thread gravel bed rivers. J. Geophys. Res. Earth Surf., 112 https://doi.org/10.1029/2006JF000549.

Pearson, A.J., Snyder, N.P., Collins, M.J., 2011. Rates and processes of channel response to dam removal with a sand-filled impoundment. Water Resour. Res., 47 https://doi.org/10.1029/2010WR009733.

Pfeiffer, A.M., Finnegan, N.J., Willenbring, J.K., 2017. Sediment supply controls equilibrium channel geometry in gravel rivers. Proc. Natl. Acad. Sci. 114, 3346–3351. https://doi.org/10.1073/pnas.1612907114.

Phillips, J.D., 1991. Multiple modes of adjustment in unstable river channel cross-sections. J. Hydrol. 123, 39–49. https://doi.org/10.1016/0022-1694(91)90067-R.

Phillips, J.D., 2009. Changes, perturbations, and responses in geomorphic systems. Progress in Physical Geography: Earth and Environment 33, 17–30. https://doi.org/10.1177/0309133309103889.

Pitlick, J., 1993. Response and recovery of a subalpine stream following a catastrophic flood. Geol. Soc. Am. Bull. 105, 657–670. https://doi.org/10.1130/0016-7606(1993)105<0657:RAROAS>2.3.CO;2.

Pitlick, J., Marr, J., Pizzuto, J., 2013. Width adjustment in experimental gravel-bed channels in response to overbank flows. J. Geophys. Res. Earth Surf. 118, 553–570. https://doi.org/10.1002/jgrf.20059.

Pizzuto, J., O'Neal, M.A., Narinesingh, P., Skalak, K., Jurk, D., Collins, S., Calder, J., 2018. Contemporary fluvial geomorphology and suspended sediment budget of the partly confined, mixed bedrock-alluvial South River, Virginia, USA. GSA Bull. 130, 1859–1874. https://doi.org/10.1130/B31759.1.

Ratcliffe, N.M., Stanley, R.S., Gale, M.H., Thompson, P.J., Walsh, G.J., 2011. Bedrock geologic map of of Vermont. U.S. Geological Survey Scientific Investigations Map. 3184 .. https://pubs.usgs.gov/sim/3184/. (Accessed August 2020).

Rathburn, S.L., Shahverdian, S.M., Ryan, S.E., 2018. Post-disturbance sediment recovery: implications for watershed resilience. Geomorphology 305, 61–75. https://doi.org/10.1016/j.geomorph.2017.08.039.

Renshaw, Carl, Magilligan, Francis, Doyle, Helen, Dethier, Evan, Kantack, Keith, 2019. Rapid response of New England (USA) rivers to shifting boundary conditions: Processes, time frames, and pathways to post-flood channel equilibrium. Geology 47 (10), 997–1000. https://doi.org/10.1130/G46702.1.

Ries III, K.G., Newson, J.K., Smith, M.J., Guthrie, J.D., Steeves, P.A., Haluska, T., Kolb, K.R., Thompson, R.F., Santoro, R.D., Vraga, H.W., 2017. StreamStats. Version 4: U.S. Geological Survey Fact Sheet USGS Numbered Series. 2017–3046. https://doi.org/10.3133/fs20173046.

Roberts, M.O., Renshaw, C.E., Magilligan, F.J., Brian Dade, W., 2020. Field Measurement of the probability of coarse-grained sediment entrainment in natural rivers. J. Hydraul. Eng., 146 https://doi.org/10.1061/(ASCE)HY.1943-7900.0001694.

Schumm, S.A., 1979. Geomorphic Thresholds: The concept and its applications. Transactions of the Institute of British Geographers. 4, pp. 485–515. https://doi.org/10.2307/622211.

Schumm, S.A., Licthy, R.A., 1963. Channel widening and flood-plain construction along cimarron river in Southwestern Kansas. USGS USGS Professional Paper. 352-D (28 p).

Simon, A., Hupp, C.R., 1987. Channel evolution in modified alluvial streams. Transportation Research Record, p. 9.

Simon, A., Hupp, C.R., 1992. Geomorphic and vegetative recovery processes along modified stream channels of West Tennessee. USGS Open-File Report. 91–502 .. https://pubs.usgs.gov/of/1991/ofr_91-502/pdf/ofr_91-502.pdf. (Accessed June 2019).

Stewart, D.P., MacClintock, P., 1970. Surficial Geologic Map of Vermont: Vermont Geological Survey. Department of Water Resources. https://dec.vermont.gov/sites/dec/files/geo/StatewidePubs/SurfMapopt.pdf. (Accessed August 2020).

Trampush, S.M., Huzurbazar, S., McElroy, B., 2014. Empirical assessment of theory for bankfull characteristics of alluvial channels. Water Resour. Res. 50, 9211–9220. https://doi.org/10.1002/2014WR015597.

Wheaton, J.M., Brasington, J., Darby, S.E., Sear, D.A., 2010. Accounting for uncertainty in DEMs from repeat topographic surveys: improved sediment budgets. Earth Surf. Process. Landf. 35, 136–156. https://doi.org/10.1002/esp.1886.

Whittaker, J.G., 1987. Sediment Transport in Step-pool Streams. In: Thorne, C.R., Bathurst, J.C., Hey, R.D. (Eds.), Sediment Transport in Gravel-Bed Rivers. John Wiley and Sons, Chichester, UK, p. 38.

Wilcock, P.R., Kenworthy, S.T., Crowe, J.C., 2001. Experimental study of the transport of mixed sand and gravel. Water Resour. Res. 37, 3349–3358. https://doi.org/10.1029/2001WR000683.

Williams, G.P., 1978. Bank-full discharge of rivers. Water Resour. Res. 14, 1141–1154. https://doi.org/10.1029/WR014i006p01141.

Wohl, E., Lane, S.N., Wilcox, A.C., 2015. The science and practice of river restoration. Water Resour. Res. 51, 5974–5997. https://doi.org/10.1002/2014WR016874.

Wohl, E.E., Anthony, D.J., Madsen, S.W., Thompson, D.M., 1996. A comparison of surface sampling methods for coarse fluvial sediments. Water Resour. Res. 32, 3219–3226. https://doi.org/10.1029/96WR01527.

Wolman, M.G., 1954. A method of sampling coarse river-bed material. Eos, Transactions American Geophysical Union. 35, pp. 951–956. https://doi.org/10.1029/TR035i006p00951.
Wolman, M.G., Gerson, R., 1978. Relative scales of time and effectiveness of climate in watershed geomorphology. Earth Surface Processes 3, 189–208. https://doi.org/10.1002/esp.3290030207.
Wolman, M.G., Leopold, L.B., 1957. River floodplains: some observations on their formation. USGS Professional Paper Professional Paper. 282–C (30 p).
Wolman, M.G., Miller, J.P., 1960. Magnitude and frequency of forces in geomorphic processes. The Journal of Geology 68, 54–74.